

*Original Article*

## Synthesis and characterization of zinc doped beryllium oxide: Ethylene glycol nanofluids

P. Prakash<sup>1</sup>, J. Catherine Grace John<sup>2</sup>, T. Merita Anto Britto<sup>3</sup>, S. Rubila<sup>4</sup>,  
and A. Kingson Solomon Jeevaraj<sup>1\*</sup>

<sup>1</sup> *Department of Physics, LRG Government Arts College for Women,  
Tirupur, Tamil Nadu, 641604 India*

<sup>2</sup> *Department of Mathematics, Karunya Institute of Technology and Sciences,  
Coimbatore, Tamil Nadu, 641114 India*

<sup>3</sup> *Department of Physics, Ananda College, Devakottai, Sivagangai, Tamil Nadu, 630303 India*

<sup>4</sup> *Department of Food technology, Sri Shakthi Institute of Engineering and Technology,  
Coimbatore, Tamil Nadu, 641062 India*

Received: 14 January 2022; Revised: 2 March 2022; Accepted: 22 April 2022

### Abstract

The current study used ultrasound-assisted chemical precipitation to create zinc doped beryllium oxide (BeO) nanoparticles. X-ray diffraction (XRD) and scanning electron microscopy (SEM) were used to characterize the synthesized samples. The effect of sonication on the size of zinc-doped BeO nanoparticles is discussed. The presence of zinc-doped BeO nanoparticles with an average crystallite size of 17.89 nm was established by X-ray diffraction. The FTIR peaks at 434.97 cm<sup>-1</sup> and 1,110.08 cm<sup>-1</sup> confirm Zn and Be in them. Sonication was used to disperse the nanoparticles in ethylene glycol, resulting in a nanofluid. The nanofluids were prepared in six concentrations from 0.0005 to 0.0030 wt% and characterized by ultrasound velocity and Fourier transform infrared (FTIR) spectroscopy as well as photoluminescence. Ultrasonic studies and FTIR analysis confirmed the absence of particle–fluid interactions. The maximum intensity was at 510 nm wavelength in the photoluminescence spectra, giving the electron transition energy. Thermal conductivity and viscosity revealed an optimum concentration at 0.0025 wt% zinc-doped BeO in ethylene glycol nanofluid, for maximal heat transfer with the highest thermal conductivity of 0.265 W/mK.

**Keywords:** BeO nanoparticle, Sonication, beryllium sulphate, crystallinity index

### 1. Introduction

Nanomaterials have made tremendous progress in recent years due to their unique electrical, optical, magnetic, mechanical, and chemical capabilities, which differ greatly from those of larger particles (Loong, Salleh, Khalid, & Koteh, 2021; Mwafy, Mostafa, Awwad, & Ibrahim, 2021; Shi & Cheng, 2020). Metal oxide nanoparticles, in particular,

have attracted the attention of researchers in a variety of fields due to their distinct physical and chemical properties (Dag, Akcay, Koteh, & Guner, 2019; Morris, Farrell, & Tabor, 2019; Shah, Koteh, & Ali, 2020; Shao, Hanaor, Shen, & Gurlo, 2020). A nanoparticle is, in theory, any collection of atoms bonded together with a structural radius of 1–100 nm. This may include, for example, fullerenes, metal clusters (metal atom agglomerates), large molecules such as protein, or even water molecules as hydrogen bonded composites, which are available in water at room temperature. Nanoparticles have a large specific surface area with a large fraction of the

\*Corresponding author

Email address: drkingson.a@gmail.com

atoms at the surface. These are the main characteristics of nanoparticles, while also size, form, composition, morphology, and crystalline phase are factors that must be considered (Jamkhande, Ghule, Bamer, & Kalaskar, 2019; Saleh, 2020).

During the previous two decades, nanofluids have been drawn to the attention of investigators looking for better heat transfer liquids (Ma, Guo, Lin, & Wang, 2021; Molana & Wang, 2020; Rafiq, Shafique, Azam, & Ateeq, 2021). Nanofluids include appropriately distributed nanoparticles as opposed to the conventional liquid-solid suspensions. A large, specified region, strong dispersion stability, reduced pumping power, a reduction in particle clogging, elastic characteristics, heat conductivity, and surface wettability, are benefits of well-dispersed suspension in a base fluid (Amalraj & Michael, 2019). Nanofluids are used in many different industries. Nanofluids, for example, may cool car engines and devices with a high heat flux like high-performance microwaves, and laser diodes with high output power. Nanofluid cooling can also flow via the microscopic tiniest passageways in microelectromechanical systems to enhance effectiveness (Mallikarjuna, Reddy, Reddy, & Kumar, 2021). The globe is experiencing a severe energy problem as a result of the fast increases in both population and industrial production. Fuel use is on the rise, while supply is on the decline. As a result, the majority of countries have begun to investigate solar energy as a source of both power and heat.

Most operations, such as a power source, heating of the water, and heating and cooling, can rely on solar energy, and it has potential for specialized industrial uses (Gordeeva *et al.*, 2021; Malinowski, Leon, & Abu-Rub, 2019; Prajapati *et al.*, 2021). Despite its low energy density and sporadic nature, solar power has grown in popularity as one of the most extensively utilized alternative energy sources. It can be captured and properly stored. It might be gathered using various collectors, performing two types of conversion: photovoltaic or solar thermal. Solar energy is converted into electrical energy in the photovoltaic technique, whereas solar energy is converted into thermal energy in the thermal approach. Even photovoltaic systems have drawbacks as they require some amount of solar energy for power production, but then remains waste heat contributing to decreased productivity. To stay away from this, nanofluids are permitted to circulate through the system, which regulates the waste heat generated during the operation, resulting in greater effectiveness of electricity production (Olabi *et al.*, 2021; Sayed *et al.*, 2021; Sheikholeslami, Farshad, Ebrahimpour, & Said, 2021). Recent research has greatly enhanced solar panel manufacturing by incorporating this cooling procedure in photovoltaics with improved electrical efficiency attributes.

To enhance the performance of solar energy systems, heat transport is the most crucial factor to consider. With improved thermal and physical qualities, nanofluids are able to achieve this. Nanoparticles suspended in a base fluid are used to make solar nanofluids employed in other solar technologies, including solar cooling systems, solar panels, solar cells, and other solar devices that benefit from functional nanofluids. The increased thermal conductivity of nanofluids with nanoparticles is one of its advantages. It has a large interfacial surface area, which helps to boost heat capacity. It also has a high absorption rate and a low emittance. Nanofluids, in comparison to other macro or microparticle

suspensions, prevent sedimentation and clogging (Gupta, Singh, Kumar, & Said, 2017; Sriharan, Harikrishnan, & Ali, 2021; Tang, Hong, Jin, & Xuan, 2019; Xian, Sidik, & Najafi, 2019). Using nanofluids in solar panels has recently been the subject of research. Al<sub>2</sub>O<sub>3</sub> and TiO<sub>2</sub> (4:3 wt%) dispersed oxide particles were described in nanofluids (Masuda, Ebata, & Teramae, 1993) with 32 and 11% improvements in thermal conductivity, respectively. Al<sub>2</sub>O<sub>3</sub> (38.5 nm) and CuO (23.6 nm) nanoparticles were dispersed in water and ethylene glycol (EG)-based nanofluids (Lee, Choi, Li, & Eastman, 1999). Beryllium oxide (BeO) doped with zinc is a non-flammable hygroscopic white compound. The structure is cubic and is used in ray cell tubes, crown glass, and catalysts. Zn-doped BeO is an n-type semiconductor (Dehaghani *et al.*, 2020), both highly conductive and over a wide range. Because they are used in various fields such as coating, crowning glass production, and catalytic applications, Zn-doped BeO nanoparticles are of interest.

Most metal oxide nanoparticles have been synthesized by a variety of methods like chemical precipitation, ball milling, pyrolysis, sol-gel, or co-precipitation. There is a tetragonal crystal phase structure in Zn-doped Beryllium oxide nanoparticles (Altunal *et al.*, 2018; Britto & Jeevaraj, 2020; Gopalakrishnan & Jeevaraj, 2014). The control of particle shape of Zn-doped BeO requires various synthesis methods with different precursors. The most common method to synthesize the nanoparticles is by chemical precipitation. However, no reports are available on synthesis of Zn-doped BeO nanoparticles by chemical precipitation. In addition, this is the first report showing ultrasound-assisted synthesis of Zn-doped BeO: Ethylene glycol nanofluids.

Nanofluids are usually produced via a two-step technique that is the most cost-effective means of producing them in large scale. A two-stage approach was also employed in this investigation. In this work, Zn-doped BeO nanoparticles were dispersed in ethylene glycol with the aid of an ultrasonic processor. Six distinct concentrations (0.0005, 0.0010, 0.0015, 0.0020, 0.0025, 0.0030) wt% of Zn-doped BeO:EG nanofluids were prepared. At 0.0025 wt% the thermal conductivity of newly formulated Zn-doped BeO in ethylene glycol nanofluid reached its maximum, making this particular concentration the most suitable for heat transfer applications. The graph reveals that 0.0025wt% Zn-doped BeO in ethylene glycol nanofluid system is optimal for heat transfer applications with the highest 0.265 W/mK thermal conductivity. So, this study has confirmed that the synthesized Zn-doped BeO: EG nanofluids are suitable for conventional heat transfer applications.

## 2. Materials and Methods

### 2.1 Chemical reagents

In the chemical precipitation method, the objective is to separate the solids from the liquid. Through the chemical precipitation method, we can synthesize zinc doped beryllium oxide nanoparticles from beryllium sulfate (BeSO<sub>4</sub>·4H<sub>2</sub>O), zinc nitrate (Zn(NO<sub>3</sub>)<sub>2</sub>), and sodium hydroxide (NaOH). Analytical reagent grade chemicals were used in the experiment without further purification. Deionized water was used throughout the experiment for preparing solutions.

## 2.2 Synthesis of Zn-doped BeO nanoparticles

The precursor used was beryllium sulphate tetrahydrate. First, it was dissolved in 50 ml distilled water to 0.8 M concentration and then 0.2 M zinc nitrate was dissolved in 50 ml of distilled water. Then both the prepared solutions were added together under mixing with a magnetic stirrer for a few minutes. Next, 2.5 M concentration NaOH was dropped slowly for three hours to have a good precipitate. The solution was then subjected to sonication using an ultrasonicator for 45 minutes, so that the particles were dispersed well. The ratio of 1:2.5 M solution was prepared. The white precipitate was obtained and kept undisturbed for 12 hours. The precipitate formed was filtered. It was washed with deionized water several times, then dried at 60°C for 24 hours, and annealed at 840°C. The final product was Zn-doped BeO nanoparticles.

## 2.3 Preparation of nanofluids

Nanofluids are usually produced via a two-step technique that is the most cost-effective means for large-scale production. A two-stage approach was also employed in this investigation. In this work, Zn-doped BeO nanoparticles were dispersed in ethylene glycol with the aid of an ultrasonic processor. Six distinct concentrations (0.0005, 0.0010, 0.0015, 0.0020, 0.0025, 0.0030) wt% of Zn-doped BeO:EG nanofluids were prepared.

## 2.4 Characterizations

The phase fraction and crystallite size in the samples were determined using a SHIMADZU 6000 X-ray diffractometer with 0.154 nm Cu-K radiation source in the range from 20° to 80°. The surface morphology was studied using a JEOL/JSM 6390 scanning electron microscope (SEM). An ALPHA-ECO-ATR/BRUKER Fourier transform infrared spectrometer was used to investigate the molecular interactions. For Zn-doped BeO nanofluids, thermal conductivity was measured in KD2 pro thermal property analyzer from Decagon Devices, USA, Inc., and viscosity studies were carried out using a Brookfield viscometer. Ultrasonic studies were performed with the help of a digital pulse-echo velocity meter (VCT-70A) at the fixed 2MHz frequency.

## 3. Results and Discussion

### 3.1 XRD analysis of Zn-doped BeO nanoparticles

The XRD pattern of zinc doped BeO nanoparticles is shown in Figure 1. For the Zn-doped BeO nanoparticles, the XRD pattern reveals the presence of precursor sulfate. The XRD peaks confirmed the production of Zn-doped BeO in hexagonal phase, which agrees well with JCPDS 350818. The (100), (002), and (101) planes of Zn-doped BeO nanoparticles are ascribed to the characteristic's peaks at 38.294°, 41.429°, 43.786°. The firm peaks show that the crystalline size is prominent (Altunal *et al.*, 2020; Chanthima, Sangwaranatee, & Kaewkhao, 2016; Trivedi *et al.*, 2018). The ultrasonication achieved good crystallinity.

The Debye-Scherer equation was used to estimate the crystalline size in Zn-doped BeO nanoparticles based on XRD data.

$$D = \frac{k\lambda}{\beta \cos \theta} \quad (1)$$

Here D is the size of crystallite in nm,  $\lambda$  is the wavelength of X-ray source (1.54 Å),  $k$  is a shape constant (0.94),  $\beta$  is the full-width half-maximum in radians, and  $\theta$  is the Bragg diffraction angle of the XRD peak. Zn-doped BeO was calcined at 840°C. The crystallite size was determined using data acquired from the dominant peaks for (100), (002), and (101) orientations. X-ray diffraction studies confirmed the presence of Zn-doped BeO nanoparticles with an average crystallite size of 17.89 nm.

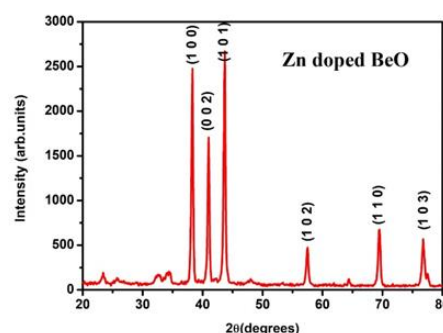


Figure 1. XRD pattern of Zn-doped BeO nanoparticles calcined at 840°C

### 3.2 SEM analysis of Zn-doped BeO nanoparticles

Figure 2 (a) and (b) show SEM images of Zn-doped BeO nanoparticles at the magnifications 30,000 and 55,000. From the SEM images of Zn-doped beryllium oxide, it was observed that the particles are well dispersed and hexagonal, as the specific uniform crystalline structure for this sample was calcined at 840°C.

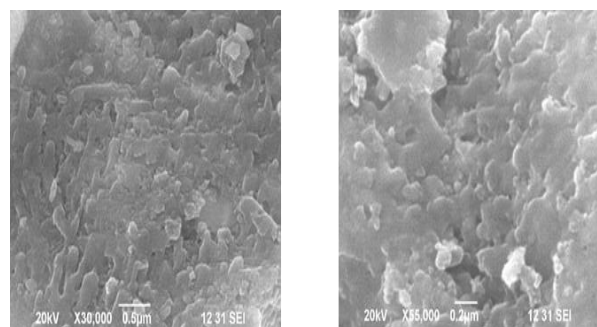


Figure 2. (a) and (b): SEM images of Zn-doped BeO nanoparticles

### 3.3 FTIR analysis of Zn-doped BeO nanoparticles

The Zn-doped BeO nanoparticles were measured over the 500-4000  $\text{cm}^{-1}$  range in the FTIR spectra and a

beryllium peak was found to be bonded firm. The peaks were compared with the standard IR datasheet confirming the prepared nanomaterials and showing that the bond was stretching in Figure 3. The first absorption peak at  $434.97\text{cm}^{-1}$  indicates Zn. Corresponding peak for sulfate is at  $622.07\text{cm}^{-1}$ , beryllium at  $1,110.08\text{cm}^{-1}$ , and O-H at  $3,376.54\text{cm}^{-1}$ . All vibrational peak modes (Roedel, Urakawa, Kureti, & Baiker, 2008) were found.

### 3.4 Photoluminescence (PL)

This was analyzed for the prepared nanoparticles of Zn-doped BeO, and the maximum intensity was observed at 510 nm wavelength. This gives the electron transition energy level in the material (Olesiak-Banska, Waszkielewicz, Obstarczyk, & Samoc, 2019). The significant peak with its intensity is shown in Figure 4.

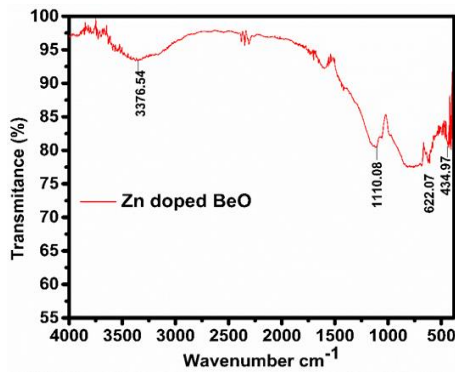


Figure 3. FTIR spectrum of Zn-doped BeO nanoparticles

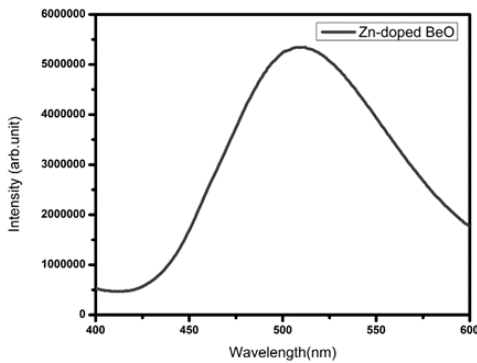


Figure 4. The photoluminescence peak of Zn doped BeO nanoparticles

#### 3.4.1 Ultrasonic velocity study of Zn-doped BeO: ethylene glycol nanofluids

The measurements were done at 313K temperature for the six concentrations (0.0005, 0.0010, 0.0015, 0.0020, 0.0025, and 0.0030 wt%). The density measurements were carried out using a specific gravity bottle. Acoustical parameters were calculated (Sundharam, Jeevaraj, & Chinnusamy, 2017) using the experimentally determined values of density ( $\rho$ ) and ultrasonic velocity ( $v$ ).

The curve exhibits linear velocity dependence on concentration, indicating that the nanofluid system does not have significant particle-fluid interactions, instead the Zn-doped BeO nanoparticles are steadily suspended in the base fluid. A reduction in the acoustic speed with Zn-doped BeO content was observed. The non-linear velocity change in the curve was caused by settling of Zn-doped BeO nanoparticles.

#### 3.4.2 Ultrasonic velocity ( $v$ )

To define ultrasonic velocity, we need to know how far apart particles in a fluid are moving with regard to time.

$$(v) = f\lambda \quad (2)$$

The variables are:  $v$  for velocity;  $f$  for frequency; and  $\lambda$  for wavelength.

#### 3.4.3 Adiabatic compressibility ( $\beta$ )

The compressibility of a fluid is an essential physical quantity in fluid mechanics. It is determined by the fluid's structure. There are two types of compression: isothermal or isentropic compressibility (adiabatic compressibility). Isentropic (adiabatic) compressibility may be obtained by ultrasonic techniques when acoustic waves travel across the medium. The electrostatic field created by interacting atoms in a fluid medium impacts the molecular arrangement, which can greatly affect the adiabatic compressibility (Premalatha & Jeevaraj, 2018). The adiabatic compressibility may be calculated from known density ( $\rho$ ) and ultrasonic velocity ( $v$ ) of the nanofluid.

$$(\beta) = \frac{1}{\rho v^2} \quad (3)$$

#### 3.4.4 Specific acoustic impedance ( $Z$ )

The ratio of acoustic pressure to flow defines the specific acoustic impedance. Acoustic power and intensity, as well as reflection and transmission at boundaries, may be calculated with this tool. A medium's density multiplied by the speed of sound in the medium equals its resonant frequency.

The specific acoustic impedance is given by

$$\rho^2 Z = V \quad (4)$$

Here  $\rho$  = density and  $v$  = ultrasonic velocity. Particle-fluid interactions in a nanofluid systems are shown by large fluctuations in these parameters with regard to particle concentration and temperature. In Figures 5-8, different concentrations of EG at various temperatures are shown to affect the acoustical characteristics.

The velocity of the waves was recorded in the ultrasonic investigation for six concentrations at room temperature, and the adiabatic compressibility was established utilizing the velocity and density relationship and is shown in Table 1. The greatest adiabatic compressibility was observed for the 0.0025 wt% case (Gupta, Magotra, Sandarve, & Sharma, 2015).

Table 1. Nanofluids with six particle concentrations were measured for acoustic velocity, density, adiabatic compressibility, and impedance

Concentration (mol)	Velocity V (m/s)	Density $\rho$ (Kg/m <sup>3</sup> )	Adiabatic compressibility $\beta$ (N <sup>-1</sup> m <sup>2</sup> )	Impedance Z (Kg.m <sup>-2</sup> s <sup>-1</sup> )
0.0000	1531.45	1071.98	3.9774	1641693.2
0.0005	1536.29	1072.03	3.9522	1646965.9
0.0010	1534.21	1072.09	3.9627	1644815.9
0.0015	1534.85	1072.14	3.9592	1645583.0
0.0020	1533.52	1072.19	3.9659	1644233.6
0.0025	1536.98	1072.24	3.9478	1648029.8
0.0030	1532.83	1072.29	3.9691	1643652.3

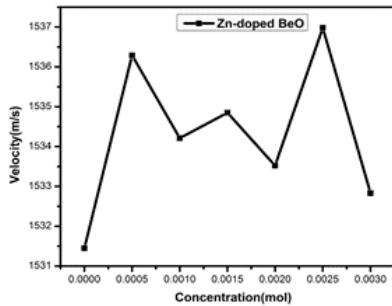


Figure 5. The acoustic velocity depends on particle concentration

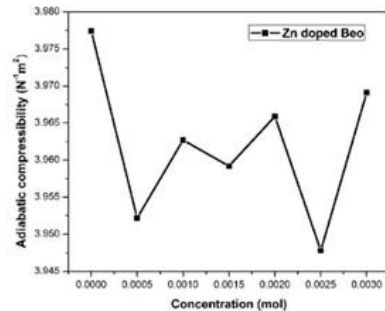


Figure 7. The adiabatic compressibility as function of concentration

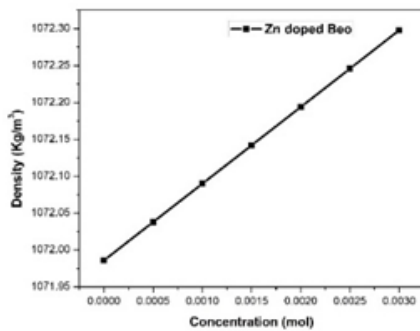


Figure 6. The density as function of concentration

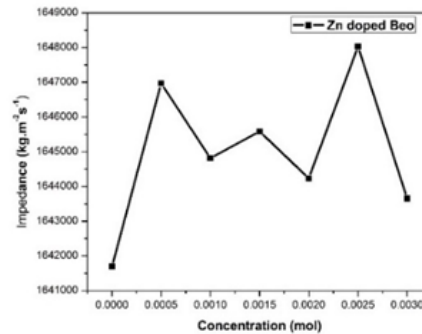


Figure 8. The impedance as function of concentration

### 3.4.5 Thermal conductivity analysis of Zn-doped BeO: ethylene glycol nanofluids

The variation of thermal conductivity with the concentration of Zn-doped BeO: ethylene glycol nanofluid system is shown in Figure 9. The nanofluids show non-linear decrease of the thermal conductivity up to a certain concentration. Nanomaterial effects mainly depend on the size of the particles. For an accurate measurement of the thermal properties of a liquid sample, the sample must still be in contact with the sensor until the readings are completed. Figures 5-8 show the graphs for the various concentrations. As concentration was increased to 0.0030 wt% the system showed decreasing thermal conductivity due to structural changes in the nanofluid (Gupta, Magotra, Sandarve, & Sharma, 2015). At 0.0025 wt%, the thermal conductivity reached its maximum, which makes this particular concentration the most suitable for heat transfer applications. The graphs reveal that 0.0025wt% Zn doped BeO in ethylene glycol nanofluid system was optimal for heat transfer applications, with the highest 0.265 W/mK thermal conductivity.

### 3.4.6 Viscosity Studies of Zn-doped BeO: ethylene glycol nanofluids

The viscosity is a significant and essential characteristic of all fluid types, indicating the resistance of a fluid against deformation by shear stress. The consistency has a considerable effect on the rheological and thermal behaviors of nanofluids. The viscosity is a measure of the friction between fluid molecules, and the contact surface of nanoparticles plays a crucial role in fluid flow and heat transfer phenomena (Prasher, Song, Wang, & Phelan, 2006). Table 2 shows viscosity at the various concentrations of the prepared nanofluids. The viscosity decreased with concentration of Zinc doped BeO in the nanofluid, as shown in Figure 10.

## 4. Conclusions

Ultrasound assisted chemical synthesis was used to make Zn-doped BeO nanoparticles. The nanostructures were hexagonal in form according to SEM imaging. An XRD pattern disclosed the nanostructure of the produced

Table 2. Nanofluids with six particle concentrations were measured for thermal conductivity.

Concentration (mol)	Thermal Conductivity(W/m.K)
0.0000	0.258
0.0005	0.254
0.0010	0.261
0.0015	0.255
0.0020	0.257
0.0025	0.265
0.0030	0.252

Table 3. Nanofluids with six particle concentrations were measured for viscosity

Molar concentration (mol)	Viscosity (cP)
0.0000	14.6
0.0005	14.2
0.0010	13.9
0.0015	14.7
0.0020	13.6
0.0025	13.7
0.0030	13.5

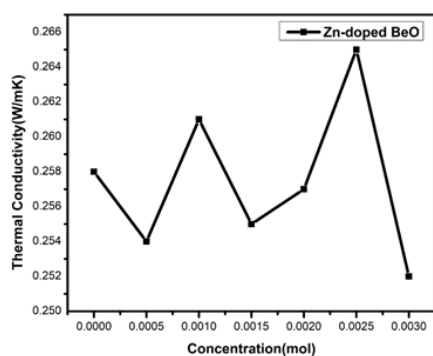


Figure 9. The thermal conductivity as function of concentration

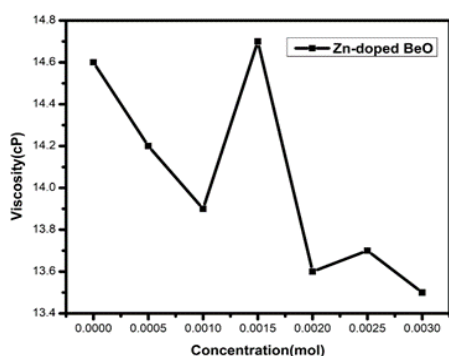


Figure 10. The viscosity as function of concentration

nanoparticles and found the average crystallite size as 17.89 nm. The crystalline nature of the nanoparticles was indicated by the crystallinity index of the Zn-doped BeO nanoparticles (1.69). The FTIR peaks at  $434.97\text{ cm}^{-1}$  and  $1110.08\text{ cm}^{-1}$  confirmed the presence of Zn and Be in the nanoparticles. The

sonication regulates the size of the Zn-doped BeO nanoparticles during synthesis. Zn doped BeO: ethylene glycol nanofluids of six concentrations were synthesized by a two-step method. Ultrasound velocity and FTIR spectra confirmed the absence of particle-fluid interactions in the nanofluids. Thermal conductivity and viscosity measurements revealed the heat transfer efficiency of the nanofluids. The results indicate that 0.0025 wt% of Zn doped BeO in ethylene glycol nanofluid is suitable for conventional heat transfer applications.

### Acknowledgements

Authors thankfully acknowledge the provision of characterisation facilities by the Karunya Institute of Science and Technology, Coimbatore, Tamil Nadu.

### References

- Abbott, W. S. (1925). A method of computing the effectiveness of insecticide. *Journal of Economic Entomology*, 18, 265-267. doi:10.1093/jee/18.2.265a
- Altunal, V., Guckan, V., Yu, Y., Dicker, A., & Yegingil, Z. (2020). A newly developed OSL dosimeter based on beryllium oxide: BeO: Na, Dy, Er. *Journal of Luminescence*, 222, 117140. doi:10.1016/j.jlum.2020.117140
- Altunal, V., Yegingil, Z., Tuken, T., Depci, T., Ozdemir, A., Guckan, V., . . . Bulur, E. (2018). Optically stimulated luminescence characteristics of BeO nanoparticles synthesized by sol-gel method. *Radiation Measurements*, 118, 54-66. doi:10.1016/j.radmeas.2018.08.009
- Amalraj, S., & Michael, P. A. (2019). Synthesis and characterization of Al<sub>2</sub>O<sub>3</sub> and CuO nanoparticles into nanofluids for solar panel applications. *Results in Physics*, 15, 102797. doi:10.1016/j.rinp.2019.102797
- Britto, T., & Jeevaraj, A. (2020). Acoustical studies on beryllium oxide/silicone oil nanofluids. *Sensor Letters*, 18(1), 69-73. doi:10.1166/sl.2020.4191
- Chanthima, N., Sangwanate, N., & Kaewkhao, J. (2016). The study of physical and optical properties of Barium Borophosphate glasses. *Materials Science Forum*, 872, 128-132. doi:10.4028/www.scientific.net/msf.872.128
- Dag, M., Akcay, N., Koten, H., & Guner, K. (2019). Determination of photovoltaic properties for nanostructures. *Journal of Electronic Materials*, 48(11), 6919-6931. doi:10.1007/s11664-019-07380-7
- Dehaghani, M. Z., Mashhadzadeh, A. H., Salmankhani, A., Karami, Z., Habibzadeh, S., Ganjali, M. R., & Saeb, M. R. (2020). Fracture toughness and crack propagation behavior of nanoscale beryllium oxide graphene-like structures: A molecular dynamics simulation analysis. *Engineering Fracture Mechanics*, 235, 107194. doi:10.1016/j.engfracmech.2020.107194

- Gopalakrishnan, M., & Jeevaraj, A. K. S. (2014). Template-free solvothermal synthesis of copper oxide nanorods. *Materials Science in Semiconductor Processing*, 26, 512-515. doi:10.1016/j.mssp.2014.05.045
- Gordeeva, L. G., Tu, Y. D., Pan, Q., Palash, M. L., Saha, B. B., Aristov, Y. I., & Wang, R. Z. (2021). Metal-organic frameworks for energy conversion and water harvesting: A bridge between thermal engineering and material science. *Nano Energy*, 84, 105946. doi:10.1016/j.nanoen.2021.105946
- Gupta, M., Singh, V., Kumar, R., & Said, Z. (2017). A review on thermophysical properties of nanofluids and heat transfer applications. *Renewable and Sustainable Energy Reviews*, 74, 638-670. doi:10.1016/j.rser.2017.02.073
- Gupta, V., Magotra, U., Sandarve, S. A., & Sharma, M. (2015). CuO nanofluids: particle-fluid interaction study using ultrasonic technique. *Journal of Chemical and Pharmaceutical Research*, 7, 313-326.
- Jamkhande, P. G., Ghule, N. W., Bamer, A. H., & Kalaskar, M. G. (2019). Metal nanoparticles synthesis: An overview on methods of preparation, advantages and disadvantages, and applications. *Journal of Drug Delivery Science and Technology*, 53, 101174. doi:10.1016/j.jddst.2019.101174
- Lee, S., Choi, S. S., Li, S. A., & Eastman, J. A. (1999). Measuring thermal conductivity of fluids containing oxide nanoparticles. *Journal of Heat Transfer*, 121(2), 280-289 doi:10.1115/1.2825978
- Loong, T. T., Salleh, H., Khalid, A., & Koten, H. (2021). Thermal performance evaluation for different type of metal oxide water based nanofluids. *Case Studies in Thermal Engineering*, 27, 101288. doi:10.1016/j.csite.2021.101288
- Ma, T., Guo, Z., Lin, M., & Wang, Q. (2021). Recent trends on nanofluid heat transfer machine learning research applied to renewable energy. *Renewable and Sustainable Energy Reviews*, 138, 110494. doi:10.1016/j.rser.2020.110494
- Malinowski, M., Leon, J. I., & Abu-Rub, H. (2019). Photovoltaic energy systems. *Power Electronics in Renewable Energy Systems and Smart Grid: Technology and Applications*, 347-389. doi:10.1002/9781119515661.ch7
- Mallikarjuna, K., Reddy, Y. S., Reddy, K. H., & Kumar, P. S. (2021). A nanofluids and nanocoatings used for solar energy harvesting and heat transfer applications: A retrospective review analysis. *Materials Today: Proceedings*, 37, 823-834. doi:10.1016/j.matpr.2020.05.833
- Masuda, H., Ebata, A., & Teramae, K. (1993). Alteration of thermal conductivity and viscosity of liquid by dispersing ultra-fine particles. Dispersion of Al<sub>2</sub>O<sub>3</sub>, SiO<sub>2</sub> and TiO<sub>2</sub> ultra-fine particles. *Thermophysical Properties*, 7(4), 227-233. doi:10.2963/jjtp.7.227
- Molana, M., & Wang, H. (2020). A critical review on numerical study of nanorefrigerant heat transfer enhancement. *Powder Technology*, 368, 18-31. doi:10.1016/j.powtec.2020.04.044
- Morris, N. J., Farrell, Z. J., & Tabor, C. E. (2019). Chemically modifying the mechanical properties of core-shell liquid metal nanoparticles. *Nanoscale*, 11(37), 17308-17318. doi:10.1039/C9NR06369B
- Mwafy, E. A., Mostafa, A. M., Awwad, N. S., & Ibrahim, H. A. (2021). Catalytic activity of multi-walled carbon nanotubes decorated with tungsten trioxides nanoparticles against 4-nitrophenol. *Journal of Physics and Chemistry of Solids*, 158, 110252. doi:10.1016/j.jpics.2021.110252
- Olabi, A. G., Elsaid, K., Sayed, E. T., Mahmoud, M. S., Wilberforce, T., Hassiba, R. J., & Abdelkareem, M. A. (2021). Application of nanofluids for enhanced waste heat recovery: A review. *Nano Energy*, 84, 105871. doi:10.1016/j.nanoen.2021.105871
- Olesiak-Banska, J., Waszkielewicz, M., Obstarczyk, P., & Samoc, M. (2019). Two-photon absorption and photoluminescence of colloidal gold nanoparticles and nanoclusters. *Chemical Society Reviews*, 48(15), 4087-4117. doi:10.1039/C8CS00849C
- Prajapati, M., Shah, M., Soni, B., Parikh, S., Sircar, A., Balchandani, S., . . . Tala, M. (2021). Geothermal-solar integrated groundwater desalination system: Current status and future perspective. *Groundwater for Sustainable Development*, 12, 100506. doi:10.1016/j.gsd.2020.100506
- Prasher, R., Song, D., Wang, J., & Phelan, P. (2006). Measurements of nanofluid viscosity and its implications for thermal applications. *Applied Physics Letters*, 89(13), 133108. doi:10.1063/1.2356113
- Premalatha, M., & Jeevaraj, A. K. S. (2018). Preparation and characterization of hydroxyl (-OH) functionalized multi-walled carbon nanotube (MWCNT)-Dowtherm A nanofluids. *Particulate Science and Technology*, 36(5), 523-528. doi:10.1080/02726351.2016.1267286
- Rafiq, M., Shafique, M., Azam, A., & Ateeq, M. (2021). Transformer oil-based nanofluid: The application of nanomaterials on thermal, electrical and physico-chemical properties of liquid insulation-A review. *Ain Shams Engineering Journal*, 12(1), 555-576. doi:10.1016/j.asej.2020.08.010
- Roedel, E., Urakawa, A., Kureti, S., & Baiker, A. (2008). On the local sensitivity of different IR techniques: Ba species relevant in NO<sub>x</sub> storage-reduction. *Physical Chemistry Chemical Physics*, 10(40), 6190-6198.
- Saleh, T. A. (2020). Nanomaterials: Classification, properties, and environmental toxicities. *Environmental Technology and Innovation*, 20, 101067. doi:10.1016/j.eti.2020.101067
- Sayed, E. T., Abdelkareem, M. A., Mahmoud, M. S., Baroutaji, A., Elsaid, K., Wilberforce, T., . . . Olabi, A. G. (2021). Augmenting performance of fuel cells using nanofluids. *Thermal Science and Engineering Progress*, 25, 101012. doi:10.1016/j.tsep.2021.101012
- Shah, T. R., Koten, H., & Ali, H. M. (2020). Performance effecting parameters of hybrid nanofluids. *Hybrid nanofluids for convection heat transfer* (pp. 179-213). London, England: Academic Press. doi:10.1016/B978-0-12-819280-1.00005-7

- Shao, G., Hanaor, D. A., Shen, X., & Gurlo, A. (2020). Freeze casting: from low-dimensional building blocks to aligned porous structures-A review of novel materials, methods, and applications. *Advanced Materials*, 32(17), 1907176. doi:10.1002/adma.201907176
- Sheikholeslami, M., Farshad, S. A., Ebrahimpour, Z., & Said, Z. (2021). Recent progress on flat plate solar collectors and photovoltaic systems in the presence of nanofluid: A review. *Journal of Cleaner Production*, 293, 126119. doi:10.1016/j.jclepro.2021.126119
- Shi, Q., & Cheng, W. (2020). Free-Standing 2D Nanoassemblies. *Advanced Functional Materials*, 30(2), 1902301. doi:10.1002/adfm.201902301
- Sriharan, G., Harikrishnan, S., & Ali, H. M. (2021). Experimental investigation on the effectiveness of MHTS using different metal oxide-based nanofluids. *Journal of Thermal Analysis and Calorimetry*, 143(2), 1251-1260. doi:10.1007/s10973-020-09779-5
- Sundharam, E., Jeevaraj, A., & Chinnusamy, C. (2017). Effect of ultrasonication on the synthesis of barium oxide nanoparticles. *Journal of Bionanoscience*, 11(4), 310-314. doi:10.1166/jbns.2017.1449
- Tang, S., Hong, H., Jin, H., & Xuan, Y. (2019). A cascading solar hybrid system for co-producing electricity and solar syngas with nanofluid spectrum selector. *Applied Energy*, 248, 231-240. doi:10.1016/j.apenergy.2019.04.137
- Trivedi, M. K., Tallapragada, R. M., Branton, A., Trivedi, D., Latiyal, O., & Jana, S. (2018). Influence of biofield treatment on physical and structural characteristics of barium oxide and zinc sulfide. *Journal of Lasers, Optics and Photonics*, 2(2), 1000122.
- Xian, H. W., Sidik, N. A. C., & Najafi, G. J. J. O. T. A. (2019). Recent state of nanofluid in automobile cooling systems. *Journal of Thermal Analysis and Calorimetry*, 135(2), 981-1008. doi:10.1007/s10973-018-7477-3